JBC RESEARCH ARTICLE

The small aromatic compound SynuClean-D inhibits the aggregation and seeded polymerization of multiple α-synuclein strains

Received for publication, January 12, 2022, and in revised form, March 25, 2022 Published, Papers in Press, April 4, 2022,
https://doi.org/10.1016/j.jbc.2022.101902

Samuel Peña-Díaz[1,2,‡], Jordi Pujols[1,2,‡], Eftychia Vasili[3,4], Francisca Pinheiro[1,2], Jaime Santos[1,2], Zoe Manglano-Artuñedo[1,2], Tiago F. Outeiro[3,4,5,6], and Salvador Ventura[1,2,7,*]

From the [1]Institut de Biotecnologia i Biomedicina. Universitat Autonoma de Barcelona, Bellaterra, Spain; [2]Departament de Bioquimica i Biologia Molecular. Universitat Autonoma de Barcelona, Bellaterra, Spain; [3]Department of Experimental Neurodegeneration, Center for Biostructural Imaging of Neurodegeneration, University Medical Center Göttingen, Göttingen, Germany; [4]Max Planck Institute for Experimental Medicine, Göttingen, Germany; [5]Translational and Clinical Research Institute, Faculty of Medical Sciences, Newcastle University, Framlington Place, Newcastle Upon Tyne, Newcastle, United Kingdom; [6]Scientific Employee With a Honorary Contract at Deutsches Zentrum für Neurodegenerative Erkrankungen (DZNE), Göttingen, Germany; [7]ICREA, Passeig Lluis Companys 23, Barcelona, Spain

Edited by Wolfgang Peti

Parkinson's disease is a neurodegenerative disorder characterized by the loss of dopaminergic neurons in the substantia nigra, as well as the accumulation of intraneuronal proteinaceous inclusions known as Lewy bodies and Lewy neurites. The major protein component of Lewy inclusions is the intrinsically disordered protein α-synuclein (α-Syn), which can adopt diverse amyloid structures. Different conformational strains of α-Syn have been proposed to be related to the onset of distinct synucleinopathies; however, how specific amyloid fibrils cause distinctive pathological traits is not clear. Here, we generated three different α-Syn amyloid conformations at different pH and salt concentrations and analyzed the activity of SynuClean-D (SC-D), a small aromatic molecule, on these strains. We show that incubation of α-Syn with SC-D reduced the formation of aggregates and the seeded polymerization of α-Syn in all cases. Moreover, we found that SC-D exhibited a general fibril disaggregation activity. Finally, we demonstrate that treatment with SC-D also reduced strain-specific intracellular accumulation of phosphorylated α-Syn inclusions. Taken together, we conclude that SC-D may be a promising hit compound to inhibit polymorphic α-Syn aggregation.

Parkinson's disease (PD) is the second most prevalent neurodegenerative disorder associated with protein misfolding and aggregation after Alzheimer's disease and affects 0.5 to 1% of the population aged between 65 and 69 years, increasing to 1 to 3% of people aged over 80 years (1, 2). PD is characterized by the loss of dopaminergic neurons in the substantia nigra pars compacta, resulting in motor symptoms such as rigidity, tremor, and bradykinesia and nonmotor symptoms such as dementia (3). A major histopathological hallmark of PD is the formation of proteinaceous assemblies in the neuronal body and processes, known as Lewy bodies and Lewy neurites, respectively (4), whose primary protein component consists of aggregated forms of α-synuclein (α-Syn) (5, 6). This intrinsically disordered protein is a soluble monomer with diverse functions, like regulating synaptic vesicle release and trafficking, fatty acid binding, and neuronal survival (7). However, under pathological conditions, α-Syn misfolds and readily aggregates. The presence of altered α-Syn in the brain is a common feature of the synucleinopathies that, aside from PD, include PD with dementia, multiple system atrophy (MSA), and dementia with Lewy bodies (8).

The synucleinopathies differ in their symptomatology, progression, and affected cellular and anatomical compartments. It has been hypothesized that these differences might ultimately rely on the conformational heterogeneity of α-Syn amyloid structures (9–11), in analogy with the human prion protein, where distinct polymorphs, or strains, cause different histopathological lesion profiles, with divergent brain region distributions and clinical manifestations (12). This view is supported by a recent cryo-EM study showing that the structure of α-Syn amyloid filaments from the brains of individuals with MSA differs from those of individuals with dementia with Lewy bodies (10). The therapeutic implications of this conformational diversity are huge since molecules that efficiently block the aggregation of one α-Syn strain may not necessarily recognize another polymorph.

Recombinant soluble α-Syn forms amyloid fibrils *in vitro* that, despite differing at the atomic level from those observed in patients' brains (10), can seed the aggregation of endogenous α-Syn in cultured neuronal cells, primary cultured neurons, and animal brains (13–15). Moreover, synthetic α-Syn fibrils formed under different solution conditions exhibit different conformation, seeding activity, and neurotoxicity in cells and when inoculated in rat brains (11, 16–22). Surprisingly, despite compounds like anle138b (23, 24), squalamine (25), trodusquemine (26), BIOD303 (27), or fasudil (28) have

‡ These authors contributed equally to this work.
* For correspondence: Salvador Ventura, salvador.ventura@uab.es.

been shown to modulate α-Syn aggregation *in vitro* effectively, studies addressing the activity of small molecules on distinct α-Syn strains are still scarce (29).

In the present study, we prepared three assemblies from α-Syn monomer under different conditions. After confirming that they differ in their conformation and in their capacity to convert endogenous α-Syn into phosphorylated aggregates in a cellular model, we characterized how SynuClean-D (SC-D), a potent inhibitor of α-Syn aggregation (30), performs on top of the three polymorphs. We demonstrate that SC-D reduces amyloid formation in all the experimental conditions and disrupts the different fibrils. In addition, it reduces the seeding capacity of preformed aggregates *in vitro* and in cells. Altogether, the data converge to indicate that SC-D is active against different α-Syn fibrillar conformations, thus becoming a promising hit compound for developing a generic molecule to treat the synucleinopathies.

Results

α-Syn amyloid fibrils characterization

SC-D, (5-nitro-6-(3-nitrophenyl)-2-oxo-4-(trifluoromethyl)-1*H*-pyridine-3-carbonitrile) (Fig. S1*A*), has been previously described as an inhibitor of α-Syn aggregation, which can reduce protein misfolding cyclic amplification–induced aggregates propagation and disrupt fibrils, displaying anti-aggregation and neuroprotective activity in animal models of PD (30). However, whether the activity of this small molecule is restricted to the assemblies formed in the conditions in which we performed the screening or it can target alternative α-Syn aggregated conformations was unknown. To decipher this, we generated three distinct α-Syn assemblies in conditions that differ from those of previous assays, where we used phosphate-buffered saline (PBS). Both pH and salt concentration have been shown to influence α-Syn fibril formation (16, 31); therefore, we incubated recombinant α-Syn (70 μM) in buffer A (50 mM sodium acetate pH 5.0) and buffer B (50 mM Tris-HCl pH 7.5) to assess the effect of the pH and in buffer B and buffer C (50 mM Tris-HCl pH 7.5150 mM KCl) to test the impact of physiological salt concentration.

Kinetic analysis indicated that in the three conditions, α-Syn assembled into thioflavin-T (Th-T)-positive structures. Noticeably, α-Syn exhibited a high Th-T binding in buffer C, whereas the lowest levels of Th-T fluorescence corresponded to those attained in buffer A (Fig. 1*A*). Thus, both the pH and the salt of the solution significantly conditioned the kinetics of α-Syn amyloid formation. In contrast, the highest levels of light scattering were observed in buffer A, with buffers B and C rendering much lower and almost identical signals (Fig. 1*B*). This indicated the formation of aggregated species with poor Th-T staining in buffer A.

Proteinase K (PK) digestion of the aggregates indicated differential susceptibility to proteolysis. The species formed in buffer B were completely cut into two smaller fragments, whereas those in buffers A and C were significantly more resistant, while exhibiting different degradation profiles (Fig. 1*C*).

Low-magnification transmission electron microscopy (TEM) images of negatively stained samples evidenced that fibrillar sheet-like structures with many parallel protofilaments and rod-like assemblies coexisted with large and abundant, apparently amorphous, aggregates in buffer A. In contrast, isolated fibrils were apparent in buffer B, whereas fibrils tend to cluster into a mesh in buffer C (Fig. S2). High-magnification images revealed that the fibrillar material in the three solutions displayed different morphology, with fibrils in buffer A being mostly sheet-like, those in buffer B and C having a more canonical fibrillar appearance, those in buffer B appearing as straight, and the ones in buffer C twisted (Fig. 1, *D–F*). The width of the fibrils formed in buffers A, B, and C were 8.6 ± 1.9 nm, 14.6 ± 2.7 nm, and 11.9 ± 1.8 nm, respectively.

The secondary structure content of the samples was analyzed using attenuated total reflection Fourier-transform infrared (ATR-FTIR) spectroscopy (Fig. 1,*G–I* and Table S1). In all cases, the spectra were dominated by a band at 1624 to 1628 cm^{-1} attributed to the presence of intermolecular β-sheet structure. When comparing only the structures formed at physiological pH, buffer B favors a higher content of disorder (28%) than buffer C (23%), which might account for a higher sensitivity to proteolysis. Indeed, when we compared the resistance to chemical denaturation with 4 M urea of the two species in a kinetic assay, we observed that the fibrils formed in buffer C were clearly more stable and could not be denatured entirely in this harsh condition (Fig. S3). Overall, these results indicated that we had successfully prepared three distinct types of α-Syn fibrils from the same monomer, named here strains A, B, and C.

SC-D inhibits the aggregation of α-Syn into different strains

Once the generation of different conformations was confirmed, we examined the impact of SC-D (100 μM) in their aggregation processes. First, we confirmed that the SC-D does not exhibit absorbance in buffers A, B, and C at the excitation (450 nm) and emission (480 nm) wavelengths used to monitor Th-T fluorescence in our assays (Fig. S1*B*). Kinetic analysis indicated that SC-D exhibited a moderate impact on the formation of Th-T-positive species of strain A, reducing the fluorescence at the endpoint of the reaction by 32% (Fig. 2*A*). In contrast, the impact in light scattering was large, with 45% reduction at 340 nm (Fig. 2*A* inset). Thus, SC-D effectively inhibits the aggregation of α-Syn in buffer A. Its reduced effect on Th-T fluorescence can be explained by the low dye binding of the final solution, likely because of the presence of amorphous aggregates coexisting with fibrils. TEM images confirmed a reduction in the number and size of the aggregates in the presence of SC-D (Fig. 2*G*) when compared with the control samples (Fig. 2*D*).

SC-D was very effective at inhibiting the formation of α-Syn amyloid fibrils at physiological pH, both in the absence (Fig. 2*B*) and presence of salt (Fig. 2*C*), resulting in a 73% and 72% reduction of the Th-T fluorescence signal at the end of the reaction for strains B and C, respectively. In addition, light scattering measurements indicated that SC-D effectively

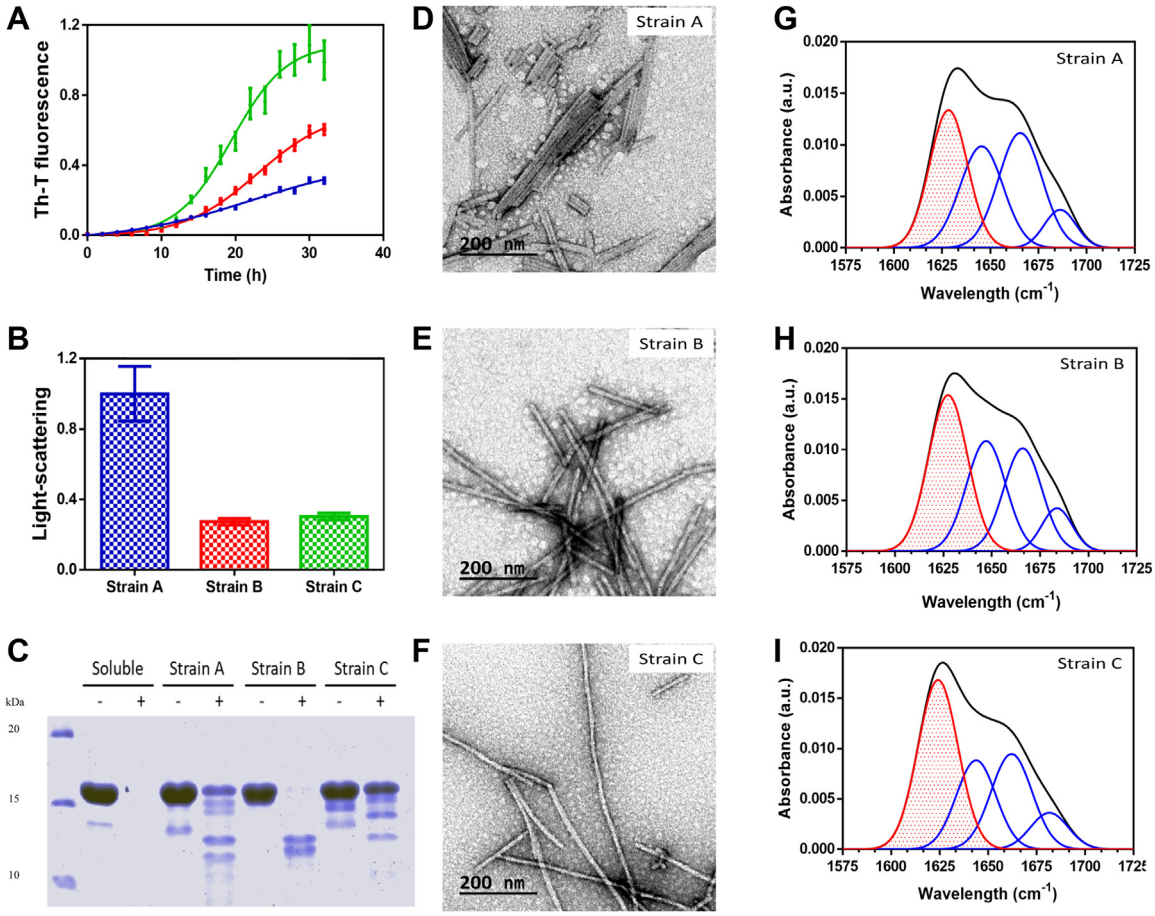

Figure 1. Strain characterization. *A*, aggregation kinetics of strain A (*blue*), strain B (*red*), and strain C (*green*). Intensity of Th-T fluorescence is plotted as normalized means in function of time and error bars as standard errors of mean. *B*, normalized light scattering measurements of final point aggregates of strain A (*blue*), strain B (*red*), and strain C (*green*). Error bars are shown as standard errors of mean values. *C*, Tricine–SDS-PAGE gels of soluble α-Syn and aggregated strains A, B, and C before (–) and after (+) PK digestion. *D–F*, representative TEM images of strain A (*D*), strain B (*E*), and C (*F*) end point aggregates. Scale bars correspond to 200 nm. *G–I*, ATR-FTIR absorbance spectra in the amide I region of final point aggregates of strain A (*G*), B (*H*), and C (*I*). α-Syn, α-synuclein; ATR, attenuated total reflectance; PK, Proteinase K; TEM, transmission electron microscopy; Th-T; thioflavin-T.

reduced the amount of aggregated material for both strains, with a decrease in the signals at 340 nm of 44% in buffer B (Fig. 2*B* inset) and 45% in buffer C (Fig. 2*C* inset). Not surprisingly, TEM images corroborated that, in both cases, the population of amyloid fibrils was significantly reduced upon SC-D treatment (Fig. 2, *H* and *I*), relative to untreated control reactions (Fig. 2, *E* and *F*). Overall, SC-D appears to act as a general inhibitor of spontaneous α-Syn aggregation.

SC-D hampers α-Syn seeded polymerization

Preformed amyloid structures, or seeds, have been shown to induce and accelerate the aggregation of the soluble protein counterpart (32). We studied the seeding capacity of the three polymorphs by adding 1% (v/v) of preformed and sonicated α-Syn fibrils formed in the same conditions followed for the correspondent assay.

No seeding capacity was observed for fibrils formed in buffer A. Nonetheless, SC-D still reduced Th-T fluorescence in 66% (Fig. 3*A*) and light scattering in 45% at 340 nm, in the presence of seeds (Fig. 3*A* inset). The highest activity of SC-D in the seeded reaction, relative to the spontaneous one, is puzzling and might indicate that despite the two processes are kinetically similar, they might involve different species for which SC-D has a distinct affinity.

Strain B seeds were very effective, abrogating the lag phase of the aggregation process and inducing a faster reaction. SC-D did restore the sigmoidal shape of the unseeded reaction but significantly reduced its speed and the final amount of Th-T-positive species by 40% (Fig. 3*B*). In addition, light scattering in the presence of the molecule was reduced in 38% at 340 nm (Fig. 3*B* inset) and thus to a lower extent than in the spontaneous reaction.

Strain C fibrils effectively seeded the soluble protein aggregation, shortening the lag phase and promoting a significantly faster reaction, which still displayed a sigmoidal shape. SC-D is exceptionally active in this condition, abrogating almost entirely α-Syn aggregation, with an 86% reduction in the final Th-T fluorescence (Fig. 3*C*). Consistently, the impact in light scattering in the seeded reaction was also very high, with a reduction of 63% at 340 nm (Fig. 3*C* inset).

These data indicate that SC-D is a very effective inhibitor of α-Syn seeded polymerization for all the strains and in all assayed conditions. The high activity on the fibrils formed in

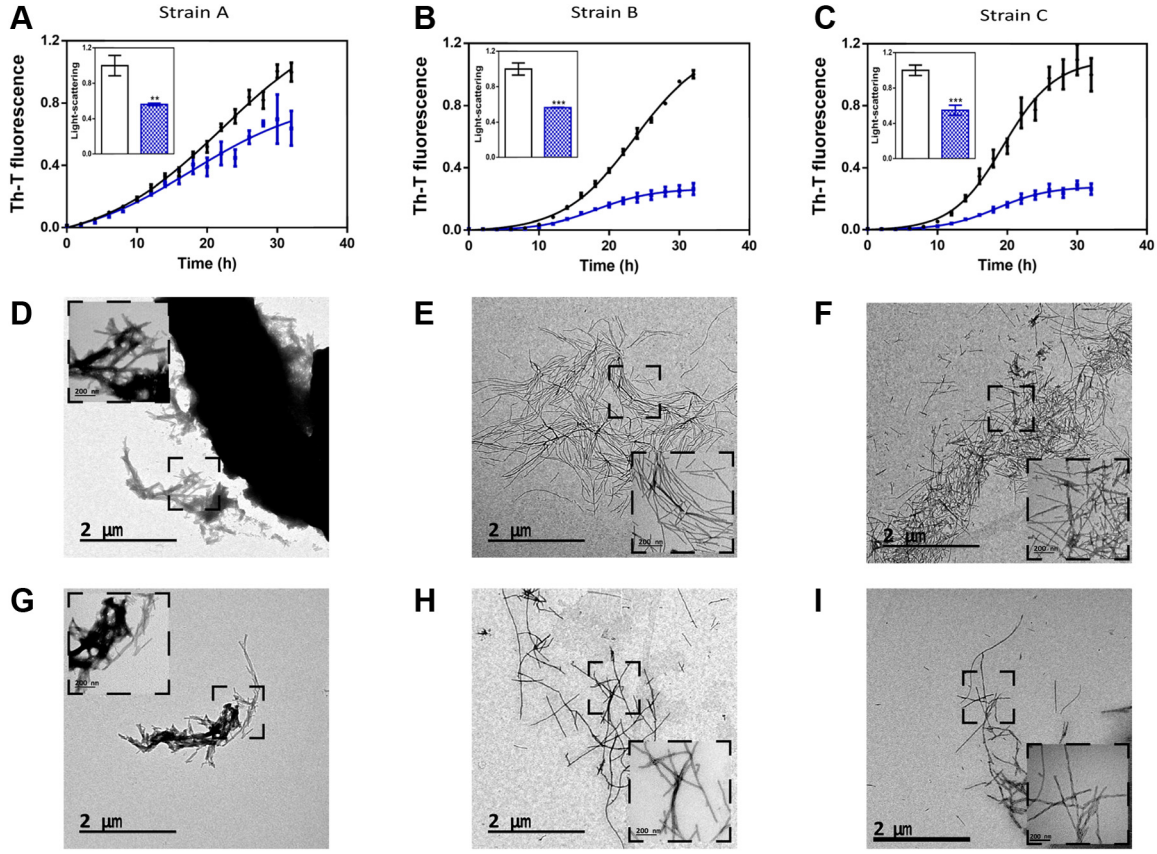

Figure 2. SynuClean-D (SC-D) effects on strain A, strain B, and strain C aggregation. *A–C*, aggregation kinetics and final point light scattering measurements (*insets*) of α-Syn in the presence (*blue*) or absence (*black*) of SC-D for strain A (*A*), strain B (*B*), and strain C (*C*). Th-T fluorescence and light scattering are plotted as normalized means. Error bars are shown as standard errors of mean values. $^{**}p < 0.01$ and $^{***}p < 0.001$. *D–I*, representative TEM images of α-Syn aggregates of strain A (*D* and *G*), strain B (*E* and *H*), and strain C (*F* and *I*), obtained in the presence (*G–I*) or absence (*D–F*) of SC-D. Scale bars correspond to 2 µm and 200 nm for main images and insets, respectively. TEM, transmission electron microscopy; Th-T; thioflavin-T.

buffer C might be related to the fact that it is the buffer that resembles more in ionic strength to the one in which we performed the initial screening, and SC-D was shown to bind preferentially to fibrillar structures in this condition.

SC-D disrupts preformed aggregates of different strains

In a previous study, SC-D evidenced fibril disaggregation capacity (30). Importantly, the compound could partially disassemble the preformed mature fibrils of the different strains formed after 48 h of incubation (Fig. 4). Strain A exhibited the highest levels of Th-T reduction after 24 h of incubation with 100 µM of SC-D (Fig. 4*A*), with a decrease of 71%. Light scattering was also reduced in 53% at 340 nm (Fig. 4*B*). This indicated that SC-D was active against both the fibrillar and nonfibrillar assemblies formed at acidic pH, which was corroborated by TEM images of SC-D-incubated samples (Fig. 4, *C* and *D*). Strain C Th-T signal decreased by 57% upon

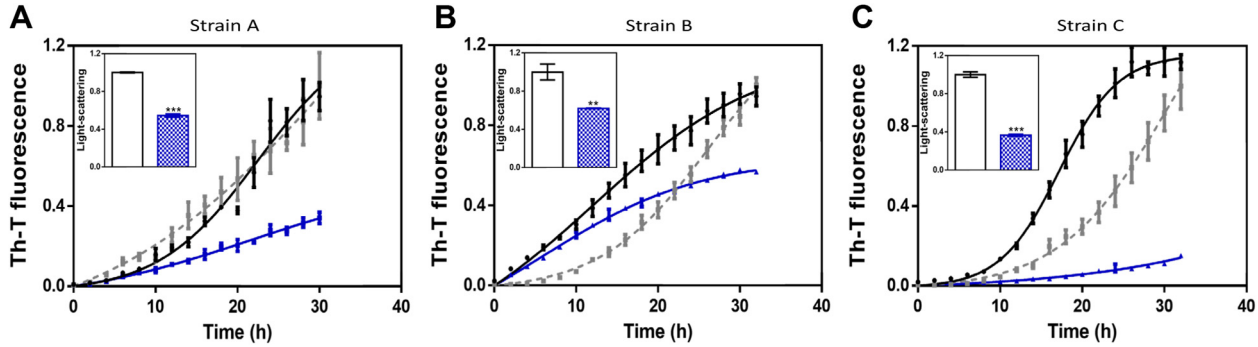

Figure 3. Seeding assays with three different strains. *A–C*, aggregation kinetics and final point light scattering measurements (*insets*) of α-Syn in buffer A (*A*), buffer B (*B*), or buffer C (*C*) in the absence of compounds and seeds (*gray dotted line*), in the presence of 1% (v/v) of preformed seeds at the specific condition (*black*), or in the presence of seeds and 100 µM of SC-D (*blue*). Th-T fluorescence is plotted as normalized means. Normalized light scattering of treated (*blue*) and untreated (*white*) seeded samples at final point for each strain is shown as inset. Error bars are shown as standard errors of mean values; $^{**}p < 0.01$ and $^{***}p < 0.001$. α-Syn, α-synuclein; SC-D, SynuClean-D.

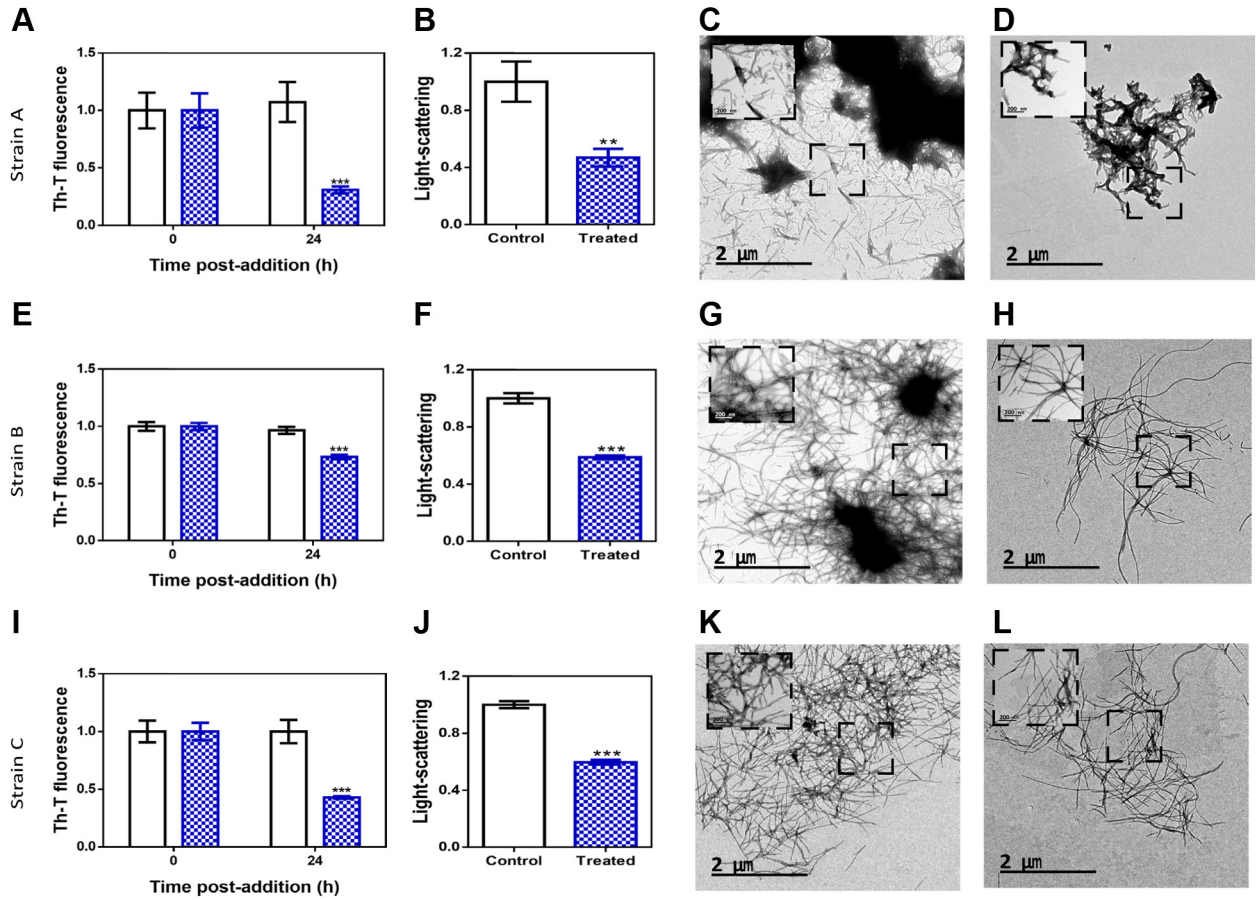

Figure 4. Disaggregational effect of SynuClean-D (SC-D). *A*, *E*, and *I*, Th-T-derived fluorescence assays before (*black*) and after (*blue*) the addition of SC-D to strain A (*A*), strain B (*E*), and strain C (*I*) preformed α-Syn fibrils. *B*, *F*, and *J*, final point light-scattering measurements in absence (*black*) and after (*blue*) the addition of SC-D to strain A (*B*), strain B (*F*), and strain C (*J*) mature α-Syn fibrils. Th-T fluorescence and light scattering are plotted as normalized means. Error bars are shown as standard errors of mean values. *C–D*, *G–H*, and *K–L*, representative TEM images of strain A (*C–D*), B (*G–H*), and C (*K–L*) aggregates in the absence (*C*, *G*, and *K*) or presence of SC-D (*D*, *H*, and *L*). Scale bars correspond to 2 μm and 200 nm for main images and insets, respectively; $^{**}p < 0.01$ and $^{***}p < 0.001$. α-Syn, α-synuclein; TEM, transmission electron microscopy; Th-T; thioflavin-T.

incubation with the molecule (Fig. 4*I*), whereas the impact on strain B was more moderate with a 27% reduction (Fig. 4*E*). Overall, the disrupting activity of SC-D on top of the different strains seems to correlate with its ability to interfere with the formation of Th-T-positive species in seeded polymerization reactions.

For both strains formed at pH 7.5, the reduction in light scattering upon SC-D addition was similar, ranging between 30 and 40% (Fig. 4, *F* and *J*). Consistently, with Th-T and light scattering data, TEM analysis of strains B and C demonstrated a significant reduction in the number of fibrils and fibril clusters for samples incubated with the molecule (Fig. 4, *H* and *L*), relative to the respective controls (Fig. 4, *G* and *K*). Overall, SC-D demonstrated significant and strain-dependent fibril dismantling activity.

α-Syn aggregates formed in the presence of SC-D show reduced seeding activity in cell culture models

We next investigated the effect of the different α-Syn fibril strains on the aggregation of endogenous α-Syn, using a stable human embryonic kidney cells 293 (HEK293) cell line that expresses α-Syn fused with enhanced green fluorescence protein (EGFP), called HEK293-α-Syn-EGFP (33, 34). In this cellular model, endogenous aggregation of α-Syn can be induced by the administration of exogenous seeds. In addition, endogenous α-Syn aggregation is accompanied by an increase in phosphorylation at serine 129 (S129), recapitulating what is observed in animal models and in the brain of patients with PD (35–38). Here, we incubated HEK293-α-Syn-EGFP cells with the different aggregated α-Syn strains, A, B, and C (100 nM), and performed immunocytochemistry (ICC) experiments with an antibody against phosphorylated α-Syn at S129 (pS129) to identify seed-promoted endogenous intracellular inclusions. The α-Syn strains were pelleted and washed with Milli Q water four times under sterile conditions; this process did not alter their physicochemical and morphological properties (Fig. S4). Then, they were diluted in PBS, sonicated, and diluted in the cell culture media and further incubated for 4 days. The same volume of PBS, buffers A, B, and C, was added to control cells.

The percentage of cells with intracellular accumulation of α-Syn-EGFP was first determined. Importantly, we did not observe any α-Syn-EGFP or pS129-positive inclusions after treatment only with PBS and buffers A, B, and C (Fig. S5). In

contrast, we found that treatment with seeds of the strain B led to a statistically significant increase of the α-Syn-EGFP inclusions compared to the cells treated with seeds of the strains A and C (Fig. 5*A*). Likewise, quantification of the pS129-positive inclusions revealed a significant increase upon treatment with strain B, whereas strains A and C did not affect the percentage of cells with pS129 inclusions (Fig. 5*A*).

These data indicate that strain B is the only one able to propagate effectively in this cell model. When the α-Syn aggregation reaction in buffer B was done in the presence of SC-D and the sample sonicated and added to the cell culture, the number of α-Syn-EGFP aggregates and especially of pS129-positive inclusions decreased significantly (Fig. 5, *A* and *B*), with respect to untreated fibrils, indicating that the molecule interfered with the exogenous seeding of intracellular α-Syn.

Discussion

Prion-like proteins can aggregate into multiple fibrillar structures. This conformational heterogeneity might explain why a single amyloidogenic protein is behind the development of disorders with diverse phenotypic traits (19, 39). As for what refers to α-Syn, evidence on structural fibrillar plasticity and its linkage to diverse synucleinopathies is progressively accumulating (13–15, 17–22). The administration of brain extracts from patients with PD or MSA into mice brains resulted in a different lesion pattern and symptomatology (40). In addition, when different recombinant α-Syn polymorphs are administered to cells and animals, the damage caused and the area of the brain that is affected vary; the different conformations, aggregation, and transmission propensity of these multiple fibrillar structures are thought to be the ultimate cause of such differential effect (9, 20). This has important implications for treating synucleinopathies since each of these disorders might need specific drugs.

Different small molecules have been described to modulate α-Syn amyloidogenesis. These include compounds that, as SC-D, interact with aggregated forms of α-Syn like anle138b, a molecule that targets oligomeric but not monomeric α-Syn (23, 24), reducing aggregation and eliciting neuroprotection in animal models of PD (41). Another class of compounds target monomeric α-Syn, such as fasudil and BIOD303, which stabilize the native protein conformation and reduce aggregation in cellular and animal models of PD (27, 28). Finally, molecules like squalamine and trodusquemine act on destabilizing α-Syn-membrane contacts and interact with the protein's negatively charged C-terminal domain (25, 26), displacing oligomeric species from cellular membranes and thus reducing their toxicity (42, 43). Furthermore, as SC-D, trodusquemine can prevent seeding-mediated aggregation of α-Syn and has shown to be effective in the same *Caenorhabditis elegans* model of PD (26). Thus, different conformations of α-Syn can now be targeted effectively, but we lack information on how the activity of these molecules depends on the aggregation conditions. In this study, we analyzed the different properties, aggregation propensities, and seeding capacity of three alternative polymorphs of α-Syn *in vitro* and in a cellular model to decipher how the activity of SC-D responds in front of different α-Syn amyloid formation scenarios.

Our study confirms a clear pH and salt dependence of the *in vitro* aggregation of α-Syn, indicating a critical role of the chemical conditions of the microenvironment surrounding the nascent aggregate. In agreement with previous data, aggregation at acidic pH is fast (44–47). This comes at the expense of the formation of abundant aggregates of lower amyloid content than at neutral pH, as deduced from Th-T, scattering, and FTIR analysis (Fig. 1 and Table S1). TEM images confirmed that short amyloid fibrils coexist with large amorphous aggregates (Figs. 1 and S2). These aggregates are significantly resistant to proteolysis but display low seeding capability *in vitro* (Fig. 3), likely due to the low proportion of ordered fibrils that can act as fibrillization nuclei. Accordingly, when exogenously applied to cells, strain A has a negligible impact on the formation of endogenous aggregated and phosphorylated α-Syn (Fig. 5). The C-terminal region of α-Syn (residues 96–140) is very acidic (10 Glu + 5 Asp), and it regulates aggregation since C-terminally truncated α-Syn aggregates faster than the full-length protein (48, 49). It is likely the impact of acidic pH in the protonation state of this region that accounts for the aggregation properties of strain A (47). SC-D

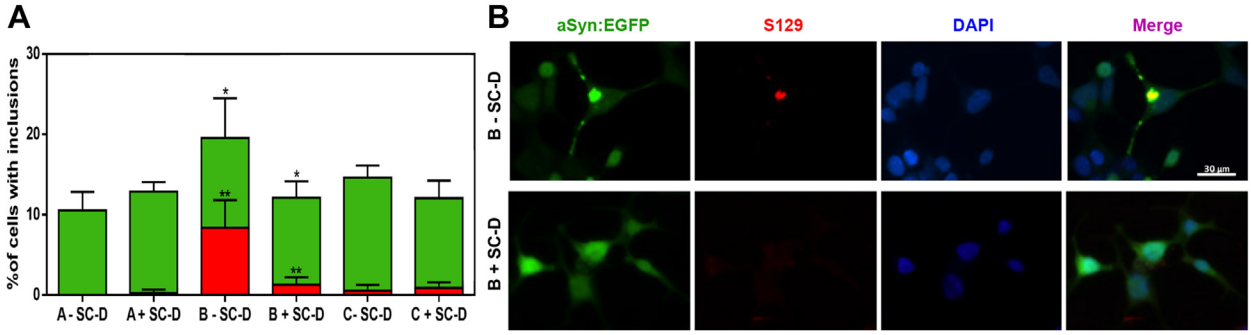

Figure 5. Effect of α-Syn strains in aggregation of endogenously expressed α-Syn-EGFP. *A*, quantification of the percentage of cells with inclusions shows that α-Syn-EGFP (*green*) and pS129 positive (*red*) inclusions are increased under treatment with strain B. Treatment α-Syn strain B with SC-D leads to a decrease in phosphorylated α-Syn inclusions (*red*) and the total level of inclusions (*green*). *B*, representative images from strain B −/+ SC-D buffer. Treatment with the α-Syn strain B-SC-D at the concentration of 100 nM for 4 days revealed the formation of α-Syn inclusions phosphorylated in S129. Representative images of cells under the treatment with B strain −/+ SC-D buffer (Scale bar 30 μm). DAPI was used for nuclear staining. Data are shown as mean ± SD (>100 cells counted per condition, four independent experiments); *$p < 0.05$ and **$p < 0.01$. α-Syn, α-synuclein; DAPI, 4′6′-diamidino-2-phenylindol; EGFP, enhanced GFP; pS129, phosphorylated S129; SC-D, SynuClean-D.

can inhibit the aggregation of α-Syn into strain A amyloid-like structures, as measured by Th-T, but it is especially active in inhibiting the formation of the predominant, amorphous, β-sheet-containing α-Syn aggregates formed at low pH as reported by light scattering and TEM data (Fig. 2). It also effectively disaggregates the mature ordered and nonordered α-Syn aggregates formed in this condition (Fig. 4). Surprisingly, SC-D is very good at inhibiting the seeded aggregation of strain A, which suggests that the species formed at pH 5.0 in the absence and presence of seeds differ conformationally and that SC-D recognizes the later ones preferentially (Fig. 3).

In contrast to pH 5.0, α-Syn aggregation at pH 7.5 results in the formation of regular amyloid fibrils with significantly higher Th-T binding and lower scattering relative to aggregates formed under acidic conditions (Fig. 1). However, the properties of these assemblies are strongly dependent on the salt content of the solution. Fibrils formed in the presence of physiological salt concentrations (strain C) display a higher β-sheet content and bind Th-T with higher affinity than those formed in its absence (strain B) (Fig. 1 and Table S1). Accordingly, strain C is significantly more resistant to proteolysis and chemical denaturation than strain B (Figs. 1 and S3). Previous studies suggested that the presence of salt induces high-level compaction of mature fibrils by hiding the C-terminal acidic domain of α-Syn (31, 50), which might account for the observed conformational and stability differences between strains B and C. The fibrils formed in both conditions seeded the *in vitro* aggregation of soluble α-Syn, but the seeding effect is more substantial for strain B, where the seeds completely abrogate the lag phase of the polymerization reaction (Fig. 3). This differential seeding capability is translated to the cellular model, with strain B significantly stimulating the aggregation of endogenous α-Syn and the accumulation of pS129 α-Syn (Fig. 5). In contrast, strain C had a lower effect on aggregation and a negligible impact on pS129 inclusion formation (Fig. 5). These properties fairly correlated with those observed when injecting α-Syn fibrils formed under the same solution conditions as our study into the striatum of mice, with the fibrils formed in the absence of KCl inducing abnormal phosphorylated α-Syn deposits through the mouse brain, whereas few pS129-positive deposits were induced by the fibrils formed in the presence of KCl (31). Salt-induced compaction and masking of the C-terminal region in strain C might explain these differences since recent studies indicate that cell surface receptors that bind α-Syn in the amyloid state to initiate cell-to-cell transmission recognize this acidic region when it is exposed at the surface of the fibrils, as it would be in strain B due to uncompensated electrostatic repulsion in the absence of salts (51). SC-D is very effective at inhibiting the aggregation of strains B and C both in the absence and the presence of seeds (Figs. 2 and 3) and acts as a fibril-disaggregating molecule for both polymorphs (Fig. 4). However, as a general trend, SC-D performs better with strain C, especially in seeded aggregation (Fig. 3), likely because the conditions in which these assemblies form resemble more in terms of salt content than those in which we performed the assay in which SC-D was initially identified. Irrespective of that, SC-D blocks the *in cell* seeding potential of strain B, decreasing the number of intracellular aggregates and, especially, of phosphorylated α-Syn inclusions (Fig. 5).

Overall, the results confirm the sensitivity of α-Syn aggregation to the solution conditions and converge to indicate that SC-D acts as a pan-inhibitor of the spontaneous and seeded formation of different α-Syn amyloid polymorphs, being able to partially disentangle them and eventually prevent the induction of intracellular aggregates by exogenous seeds. This generic property might be related to the fact that, according to previous molecular dynamic simulations (30), SC-D preferentially targets residues within (Glu61, Thr72, and Gly73) or close to (Ala53, Val55, and Thr59) the non-amyloid component domain (Fig. S6), which are expected to be relevant for α-Syn aggregation in all the assayed conditions. However, it is also clear that the activity of this molecule differs between strains, suggesting the establishment of conformation-dependent interactions with the different intermediate species. It is worth remarking that the highest SC-D activity occurs in solution conditions that resemble most those of the initial screening study, which suggests that, in principle, one can set up drug discovery assays to identify molecules that target preferentially a specific, biologically relevant, α-Syn polymorph. Meanwhile, the generic activity of SC-D positions this aromatic molecule as a hit compound from which evolve potentially active drugs for the different synucleinopathies.

Experimental procedures

Protein expression and purification

The expression and purification of α-Syn was carried out in *Escherichia coli BL21 DE3* strain as previously described (52). Briefly, *E. coli BL21* (*DE3*) containing a pET21a plasmid encoding for the α-Syn complementary DNA were grown in LB medium containing 100 μM/ml ampicillin and induced with 1 mM IPTG for 4 h at an absorbance of 600 nm of 0.6. Cells were recovered by centrifugation and washed up by resuspension and centrifugation in PBS, pH 7.4. Pellets were stored at −80 °C until used, when pellets were resuspended in 50 ml per culture liter in lysis buffer (50 mM Tris pH 8, 150 mM NaCl, 1 μg/ml pepstatin, 20 μg/ml aprotinin, 1 mM benzamidine, 1 mM PMSF, 1 mM EDTA, and 0.25 mg/ml lysozyme) and sonicated using a LABSONICU sonicator (B. Braun Biotech International). Then, sonicated samples were boiled for 10 min at 95 °C and centrifuged at 20,000*g* at 4 °C for 40 min. The soluble fraction was treated with 136 μl/ml of 10% w/v streptomycin sulfate and 228 μl/ml of pure acetic acid and centrifuged at 20,000*g* at 4 °C for 10 min. Upon centrifugation, soluble extracts were fractionated by adding 1:1 of saturated ammonium sulfate. Samples were centrifuged for 10 min at 20,000*g* and 4 °C, and the resultant pellets resuspended with 50% ammonium sulfate. After centrifugation (at 20,000*g* and 4 °C for 10 min), the pellet was resuspended in 100 mM, pH 8, ammonium acetate (5 ml per culture liter) and pure EtOH 1:1 (v/v) and harvested by centrifugation for 10 min at 20,000*g* at 4 °C. The insoluble fraction was resuspended in Tris 20 mM pH 8, filtered with a 0.22-μm filter, and

loaded into an anion exchange column HiTrap Q HP (GE Healthcare) coupled to an ÄKTA purifier high-performance liquid chromatography system (GE Healthcare). Tris 20 mM, pH 8, and Tris 20 mM, pH 8, and NaCl 1 M were used as buffer A and buffer B. αS was eluted using a using a step gradient: step 1, 0 to 20% buffer B, 5 cv; step 2, 20 to 45% buffer B, 11 cv; step 3, 100% buffer B, 5 cv. Purified αS was dialyzed against 5 L of ammonium acetate 50 mM in two steps: 4 h and overnight. The obtained protein was lyophilized and stored at −80 °C until used in the experiments.

Sample preparation

Lyophilized α-Syn was resuspended in PBS 1X to a final concentration of 210 μM and dialyzed in a 1:1000 (v/v) ratio in the presence of buffer A (50 mM sodium acetate pH 5.0), buffer B (50 mM Tris-HCl pH 7.5), or buffer C (50 mM Tris-HCl pH 7.5 supplemented with 150 mM KCl) for 24 h. Protein was filtered through a 22-μm membrane to eliminate small aggregates of α-Syn, and sample concentration was measured at 280 nm in a spectrophotometer Cary100 (Agilent) using the extinction coefficient 5960 M^{-1} cm^{-1}. SC-D (5-nitro-6-(3-nitrophenyl)-2-oxo-4-(trifluoromethyl)-1H-pyridine-3-carbonitrile) was resuspended in 100% dimethyl sulfoxide (DMSO) to a final concentration of 50 mM as preservation stock and kept stored at −20 °C. Working solutions of 4 mM SC-D in 100% were prepared for the different experiments just before use.

Protein aggregation assays

The aggregation was performed on a 96-well sealed plate, containing in each well 70 μM α-Syn (in buffer A, B, or C), 40 μM Th-T, a 1/8" diameter Teflon polyball (Polysciences Europe GmbH), and SC-D at 100 μM. Briefly, 3.75 μl of 4 mM SC-D stock was added to each well; 3.75 μl of 100% DMSO was added instead to control samples. The final volume was 150 μl (2.5% DMSO in the assay solution). The plate was fixed into an orbital Max-Q 4000 (ThermoScientific) and constantly agitated at 100 rpm and 37 °C. Th-T fluorescence was measured every 2 h by exciting through a 430- to 450-nm filter and collecting the emission signal with a 480- to 510-nm filter, using a Victor3.0 Multilabel Reader (PerkinElmer). All the assays were done in triplicate. Data were normalized and represented as mean and SEM and fitted with GraphPad Prism 6.0 software (GraphPad Software Inc) using the following equation:

$$\propto = 1 - \frac{1}{k_b(e^{k_b t} - 1) + 1}$$

accounting k_b and k_a for the homogeneous nucleation rate constant and the secondary rate constant (fibril elongation and secondary nucleation), respectively (53).

For the seeding assays, 1% (v/v) of preformed α-Syn fibrils were added to their corresponding condition after a sonication process of 5 min at intensity 9 with a Ultrasonic Cleaner sonicator (VWR International). As previously mentioned, aggregation was performed in a 96-well sealed plate, containing in each well 70 μM α-Syn (in buffer A, B, or C), 40 μM Th-T, a 1/8" diameter Teflon polyball, and SC-D at 100 μM in a total volume of 150 μl (2.5% DMSO final concentration). Control samples contained the corresponding amount of DMSO (2.5% final concentration). The plate was fixed into an orbital Max-Q 4000 (ThermoScientific) and constantly agitated at 100 rpm and 37 °C, and Th-T fluorescence measured every 2 h as previously indicated.

In the disaggregation assays, 70 μM α-Syn was incubated for 48 h at 100 rpm and 37 °C in a 96-well sealed plate, which also contains in each well 40 μM Th-T and a 1/8" diameter Teflon polyball. After 48 h, aggregated samples were exposed to 100 μM of SC-D or 2.5% of DMSO in controls. The plate was incubated for an additional period of 24 h at 100 rpm and 37 °C in an orbital Max-Q 4000, and Th-T fluorescence measured at final point as before.

TEM

Aggregated samples were diluted 1:10 in PBS 1X and softly sonicated for 5 min at intensity 2 with a Ultrasonic Cleaner sonicator (VWR International) to avoid large accumulations of fibrils. Immediately, 5 μl of the samples was placed on a carbon-coated copper grid. Grids were carefully dried 5 min later with a filter paper to remove the excess of sample and washed in Mili-Q water twice. Finally, 5 μl of 2% (w/v) uranyl acetate was added on the top of the grid for 2 min and then removed with a filter paper. Grids were left to air-dry for 10 min. Representative images were obtained screening a minimum of 30 fields per sample and using a Transmission Electron Microscopy Jeol 1400 (Peabody) operating at an accelerating voltage of 120 kV.

Light scattering

In all the assays, final-point–aggregated protein samples were carefully resuspended and recovered to measure the total aggregate formation. To a quartz cuvette, 80 μl of aggregated samples were added and excited at 340 nm to collect 90° scattering from 320 to 360 nm in a Cary Eclipse Fluorescence Spectrophotometer (Agilent).

Secondary structure determination

ATR-FTIR spectroscopy analysis of amyloid fibrils was performed using a Bruker Tensor 27 FTIR Spectrometer (Bruker Optics Inc) with a Golden Gate MKII ATR accessory. Each spectrum consists of 16 independent scans, measured at a spectral resolution of 4 cm^{-1}, within the 1800- to 1500-cm^{-1} range. Second derivatives of the spectra were used to determine the frequencies at which the different spectral components were located. Fourier-deconvolution and determination of band position of the original amide I band were performed using PeakFit software (Systat Software).

PK digestion

Eighteen microliters of aggregated α-Syn at final point was mixed with 6 μl of PK, rendering a final concentration of

5 μg/ml, and incubated for 5 min at 37 °C. Then, 8 μl of loading buffer containing 1% β-mercaptoethanol was added and the enzyme thermally inactivated for 10 min at 95 °C in a ThermoCell cooling & heating block (BIOER). Finally, 7 μl of the samples was loaded into a 12% SDS-PAGE, later stained with Blue Safe.

Mature fibril denaturation

For denaturation assays of strains B and C, 70 μM α-Syn was incubated for 48 h in the presence of DMSO and Th-T as described previously. The resultant aggregates were carefully resuspended and recovered. For chemical denaturation, 500 μl of aggregated α-Syn fibrils was mixed with 4 M urea (final concentration) in a quartz cuvette (1 ml final volume) and incubated for 2000 s at 37 °C under constant agitation (150 rpm). Meanwhile, Th-T fluorescence was recorded in a Cary Eclipse Fluorescence Spectrophotometer (Agilent) with a data pitch of 1 s using an excitation wavelength of 445 nm and recorded at 485 nm with an excitation and emission bandwidth of 2.5 and 5 nm, respectively (54). Denaturing curves were fitted to a one-step reaction using GraphPad Prism 5 (GraphPad Software).

Cell culture, cell treatment, and ICC

HEK293 stably expressing WT α-Syn fused to EGFP (HEK293- α-Syn-EGFP), under the cytomegalovirus promoter, was used for the seeding experiments (34). Cells were maintained in Dulbecco's modified Eagle's medium supplemented with 10% fetal bovine serum Gold (PAA) and 1% penicillin–streptomycin (PAN). Cells were grown at 37 °C in an atmosphere of 5% CO_2. For the seeding experiments, cells were plated on 13-mm glass coverslips in 24-well plates and incubated in 5% fetal bovine serum media. The following day, α-Syn strains were diluted in PBS, fragmented by sonication (55) and then added to cells at a final concentration of 100 nM. The fibrils were prepared in an aggregation reaction starting from 70 μM of monomeric α-Syn, in the absence or presence of 100 μM of SC-D and the corresponding proportion of DMSO for 48 h at 100 rpm and 37 °C. Preformed fibrils (PFFs) were then recovered and centrifuged at 14,000 rpm for 30 min. The supernatant was discarded, and the pellet resuspended in Milli-Q water under sterile conditions. PFFs were then centrifuged again at 14,000 rpm for 30 min, and the pellet was resuspended in Milli-Q water under sterile conditions. This step was repeated three additional times. We performed the imaging in 24-well dishes (with volume media 0.5 ml/well) and calculated to add 50 μl of PBS or PFFs (dilution 1:10). We prepared seeds by adding PFFs to sterile PBS to a final concentration of 1 μM. The minimal volume that can be used for sonication is 200 μl. We diluted 50 μl of sonicated PFFs or an equivalent volume of PBS as a control, into prewarmed cell media (1:10 dilution). We checked our PFF preparations, and we did not detect amorphous aggregates during the preparation. Control cells were exposed to vehicle only (PBS). Cells were further incubated for 4 days. ICC was carried out using standard protocols. Briefly, after treatment, the cells were washed first with PBS and then with diluted 1:10 trypsin, fixed with 4% paraformaldehyde for 20 min at room temperature (RT), permeabilized with 0.5% Triton X-100 (Sigma–Aldrich) for 20 min at RT, and blocked in 1.5% bovine serum albumin/Dulbecco's PBS for 1 h. Cells were incubated with primary antibody overnight (1:1000; anti-pS129-α-syn Rabbit Ab51253 Abcam) and secondary antibody Alexa Fluor 555 goat anti-rabbit immunoglobulin G (Life Technologies-Invitrogen) for 2 h at RT, followed by nuclei staining with 4′6′-diamidino-2-phenylindol (Sigma–Aldrich, D8417) (1:5000 in Dulbecco's PBS) for 10 min. After a final wash, coverslips were mounted by using Mowiol (Sigma–Aldrich) and subjected to fluorescence microscopy.

The proportion of cells with α-Syn inclusions within the population was then determined by counting. Each experiment was reproduced at least three independent times. Data were analyzed using a *t* test. For quantification of aggregation, at least 100 cells were counted per variant and per experiment. Images were acquired using a 63× objective lens and analyzed using LAS AF, version 2.2.1 (Leica Microsystems) software.

Statistical analysis

All graphs were generated with GraphPad Prism 6.0 software (GraphPad Software Inc). Data were analyzed by two-way ANOVA and Tukey's Honestly Significant Difference test using SPSS software, version 20.0 (IBM Analytics). All data are shown as means and SEM. $p < 0.05$ was considered statistically significant. In the graphs, *, **, and *** indicate $p < 0.05$, $p < 0.01$, and $p < 0.001$, respectively. For cellular assays, statistical analysis was done using the Student's *t* test for independent variables and the data were presented as mean ± standard deviations and represent results from at least four independent experiments.

Data availability

All data are contained within the manuscript.

Supporting information—This article contains supporting information (30).

Acknowledgments—We thank the Servei de Microscòpia at Universitat Autònoma de Barcelona for their help with TEM.

Author contributions—S. P.-D., J. P., and S. V. conceptualization; S. P.-D., J. P., E. V., F. P., J. S., and Z. M.-A. methodology; S. P.-D., J. P., E. V., S. V., and T. F. O. validation; S. P.-D. and S. V., formal analysis; S. P.-D., J. P., E. V., F. P., J. S., and Z. M.-A. investigation; S. P.-D. and S. V., writing–original draft; Z. M.-A. and S. V. supervision; T. F. O. and S. V. project administration; T. F. O. and S. V. funding acquisition.

Funding and additional information—S. V. was supported by the Spanish Ministry of Science and Innovation (PID2019–105017RB-I00), ICREA (ICREA-Academia 2015 and 2020), and the Fundación La Marató de TV3 (Ref. 20144330). T. F. O. was supported by the Deutsche Forschungsgemeinschaft (DFG, German Research Foundation) under Germany's Excellence Strategy (EXC 2067/1–390729940) and by SFB1286 (Project B8).

Conflict of interest—The authors declare that they have no conflicts of interest with the contents of this article.

Abbreviations—The abbreviations used are: α-Syn, α-synuclein; AD, Alzheimer's disease; ATR, attenuated total reflectance; DMSO, dimethyl sulfoxide; EGFP, enhanced GFP; HEK293, human embryonic kidney cells 293; ICC, immunocytochemistry; MSA, multiple system atrophy; PFF, preformed fibril; PK, proteinase K; pS129, phosphorylated S129; RT, room temperature; S129, serine 129; SC-D, SynuClean-D; TEM, transmission electron microscopy; Th-T, thioflavin-T.

References

1. Kalia, L. V., and Lang, A. E. (2015) Parkinson's disease. *Lancet* **386**, 896–912
2. Dexter, D. T., and Jenner, P. (2013) Parkinson disease: From pathology to molecular disease mechanisms. *Free Radic. Biol. Med.* **62**, 132–144
3. Marti, M. J., Tolosa, E., and Campdelacreu, J. (2003) Clinical overview of the synucleinopathies. *Mov. Disord.* **18**, S21–S27
4. Bethlem, J., and Den Hartog Jager, W. A. (1960) The incidence and characteristics of Lewy bodies in idiopathic paralysis agitans (Parkinson's disease). *J. Neurol. Neurosurg. Psychiatry* **23**, 74–80
5. Spillantini, M. G., Schmidt, M. L., Lee, V. M., Trojanowski, J. Q., Jakes, R., and Goedert, M. (1997) Alpha-synuclein in Lewy bodies. *Nature* **388**, 839–840
6. Serpell, L. C., Berriman, J., Jakes, R., Goedert, M., and Crowther, R. A. (2000) Fiber diffraction of synthetic alpha-synuclein filaments shows amyloid-like cross-beta conformation. *Proc. Natl. Acad. Sci. U. S. A.* **97**, 4897–4902
7. Bendor, J. T., Logan, T. P., and Edwards, R. H. (2013) The function of alpha-synuclein. *Neuron* **79**, 1044–1066
8. Alafuzoff, I., and Hartikainen, P. (2017) Alpha-synucleinopathies. *Handbook Clin. Neurol.* **145**, 339–353
9. Lau, A., So, R. W. L., Lau, H. H. C., Sang, J. C., Ruiz-Riquelme, A., Fleck, S. C., Stuart, E., Menon, S., Visanji, N. P., Meisl, G., Faidi, R., Marano, M. M., Schmitt-Ulms, C., Wang, Z., Fraser, P. E., *et al.* (2019) alpha-Synuclein strains target distinct brain regions and cell types. *Nat. Neurosci.* **23**, 21–31
10. Schweighauser, M., Shi, Y., Tarutani, A., Kametani, F., Murzin, A. G., Ghetti, B., Matsubara, T., Tomita, T., Ando, T., Hasegawa, K., Murayama, S., Yoshida, M., Hasegawa, M., Scheres, S. H. W., and Goedert, M. (2020) Structures of alpha-synuclein filaments from multiple system atrophy. *Nature* **585**, 464–469
11. Shahnawaz, M., Mukherjee, A., Pritzkow, S., Mendez, N., Rabadia, P., Liu, X., Hu, B., Schmeichel, A., Singer, W., Wu, G., Tsai, A. L., Shirani, H., Nilsson, K. P. R., Low, P. A., and Soto, C. (2020) Discriminating alpha-synuclein strains in Parkinson's disease and multiple system atrophy. *Nature* **578**, 273–277
12. Aguzzi, A., Heikenwalder, M., and Polymenidou, M. (2007) Insights into prion strains and neurotoxicity. *Nat. Rev. Mol. Cell Biol.* **8**, 552–561
13. Luk, K. C., Kehm, V., Carroll, J., Zhang, B., O'Brien, P., Trojanowski, J. Q., and Lee, V. M. (2012) Pathological alpha-synuclein transmission initiates Parkinson-like neurodegeneration in nontransgenic mice. *Science* **338**, 949–953
14. Luk, K. C., Kehm, V. M., Zhang, B., O'Brien, P., Trojanowski, J. Q., and Lee, V. M. (2012) Intracerebral inoculation of pathological alpha-synuclein initiates a rapidly progressive neurodegenerative alpha-synucleinopathy in mice. *J. Exp. Med.* **209**, 975–986
15. Masuda-Suzukake, M., Nonaka, T., Hosokawa, M., Oikawa, T., Arai, T., Akiyama, H., Mann, D. M., and Hasegawa, M. (2013) Prion-like spreading of pathological alpha-synuclein in brain. *Brain* **136**, 1128–1138
16. Bousset, L., Pieri, L., Ruiz-Arlandis, G., Gath, J., Jensen, P. H., Habenstein, B., Madiona, K., Olieric, V., Bockmann, A., Meier, B. H., and Melki, R. (2013) Structural and functional characterization of two alpha-synuclein strains. *Nat. Commun.* **4**, 2575
17. Gribaudo, S., Tixador, P., Bousset, L., Fenyi, A., Lino, P., Melki, R., Peyrin, J. M., and Perrier, A. L. (2019) Propagation of alpha-synuclein strains within human reconstructed neuronal network. *Stem Cell Rep.* **12**, 230–244
18. Guerrero-Ferreira, R., Taylor, N. M., Arteni, A. A., Kumari, P., Mona, D., Ringler, P., Britschgi, M., Lauer, M. E., Makky, A., Verasdonck, J., Riek, R., Melki, R., Meier, B. H., Bockmann, A., Bousset, L., *et al.* (2019) Two new polymorphic structures of human full-length alpha-synuclein fibrils solved by cryo-electron microscopy. *Elife* **8**, e56825
19. Peelaerts, W., and Baekelandt, V. (2016) a-Synuclein strains and the variable pathologies of synucleinopathies. *J. Neurochem.* **139**, 256–274
20. Peelaerts, W., Bousset, L., Van der Perren, A., Moskalyuk, A., Pulizzi, R., Giugliano, M., Van den Haute, C., Melki, R., and Baekelandt, V. (2015) alpha-Synuclein strains cause distinct synucleinopathies after local and systemic administration. *Nature* **522**, 340–344
21. Woerman, A. L., Oehler, A., Kazmi, S. A., Lee, J., Halliday, G. M., Middleton, L. T., Gentleman, S. M., Mordes, D. A., Spina, S., Grinberg, L. T., Olson, S. H., and Prusiner, S. B. (2019) Multiple system atrophy prions retain strain specificity after serial propagation in two different Tg(SNCA*A53T) mouse lines. *Acta Neuropathol.* **137**, 437–454
22. Froula, J. M., Castellana-Cruz, M., Anabtawi, N. M., Camino, J. D., Chen, S. W., Thrasher, D. R., Freire, J., Yazdi, A. A., Fleming, S., Dobson, C. M., Kumita, J. R., Cremades, N., and Volpicelli-Daley, L. A. (2019) Defining alpha-synuclein species responsible for Parkinson's disease phenotypes in mice. *J. Biol. Chem.* **294**, 10392–10406
23. Wagner, J., Ryazanov, S., Leonov, A., Levin, J., Shi, S., Schmidt, F., Prix, C., Pan-Montojo, F., Bertsch, U., Mitteregger-Kretzschmar, G., Geissen, M., Eiden, M., Leidel, F., Hirschberger, T., Deeg, A. A., *et al.* (2013) Anle138b: A novel oligomer modulator for disease-modifying therapy of neurodegenerative diseases such as prion and Parkinson's disease. *Acta Neuropathol.* **125**, 795–813
24. Dominguez-Meijide, A., Vasili, E., Konig, A., Cima-Omori, M. S., Ibanez de Opakua, A., Leonov, A., Ryazanov, S., Zweckstetter, M., Griesinger, C., and Outeiro, T. F. (2020) Effects of pharmacological modulators of alpha-synuclein and tau aggregation and internalization. *Sci. Rep.* **10**, 12827
25. Perni, M., Galvagnion, C., Maltsev, A., Meisl, G., Muller, M. B., Challa, P. K., Kirkegaard, J. B., Flagmeier, P., Cohen, S. I., Cascella, R., Chen, S. W., Limbocker, R., Sormanni, P., Heller, G. T., Aprile, F. A., *et al.* (2017) A natural product inhibits the initiation of alpha-synuclein aggregation and suppresses its toxicity. *Proc. Natl. Acad. Sci. U. S. A.* **114**, E1009–E1017
26. Perni, M., Flagmeier, P., Limbocker, R., Cascella, R., Aprile, F. A., Galvagnion, C., Heller, G. T., Meisl, G., Chen, S. W., Kumita, J. R., Challa, P. K., Kirkegaard, J. B., Cohen, S. I. A., Mannini, B., Barbut, D., *et al.* (2018) Multistep inhibition of alpha-synuclein aggregation and toxicity *in vitro* and *in vivo* by trodusquemine. *ACS Chem. Biol.* **13**, 2308–2319
27. Moree, B., Yin, G., Lazaro, D. F., Munari, F., Strohaker, T., Giller, K., Becker, S., Outeiro, T. F., Zweckstetter, M., and Salafsky, J. (2015) Small molecules detected by second-harmonic generation modulate the conformation of monomeric alpha-synuclein and reduce its aggregation in cells. *J. Biol. Chem.* **290**, 27582–27593
28. Tatenhorst, L., Eckermann, K., Dambeck, V., Fonseca-Ornelas, L., Walle, H., Lopes da Fonseca, T., Koch, J. C., Becker, S., Tonges, L., Bahr, M., Outeiro, T. F., Zweckstetter, M., and Lingor, P. (2016) Fasudil attenuates aggregation of alpha-synuclein in models of Parkinson's disease. *Acta Neuropathol. Commun.* **4**, 39
29. Peña-Díaz, S., Pujols, J., Conde-Giménez, M., Čarija, A., Dalfo, E., García, J., Navarro, S., Pinheiro, F., Santos, J., Salvatella, X., Sancho, J., and Ventura, S. (2019) ZPD-2, a small compound that inhibits α-synuclein amyloid aggregation and its seeded polymerization. *Front. Mol. Neurosci.* **12**, 306
30. Pujols, J., Pena-Diaz, S., Lazaro, D. F., Peccati, F., Pinheiro, F., Gonzalez, D., Carija, A., Navarro, S., Conde-Gimenez, M., Garcia, J., Guardiola, S., Giralt, E., Salvatella, X., Sancho, J., Sodupe, M., *et al.* (2018) Small molecule inhibits alpha-synuclein aggregation, disrupts amyloid fibrils, and prevents degeneration of dopaminergic neurons. *Proc. Natl. Acad. Sci. U. S. A.* **115**, 10481–10486
31. Suzuki, G., Imura, S., Hosokawa, M., Katsumata, R., Nonaka, T., Hisanaga, S. I., Saeki, Y., and Hasegawa, M. (2020) alpha-synuclein strains that cause distinct pathologies differentially inhibit proteasome. *Elife* **9**, e56825

32. Tornquist, M., Michaels, T. C. T., Sanagavarapu, K., Yang, X., Meisl, G., Cohen, S. I. A., Knowles, T. P. J., and Linse, S. (2018) Secondary nucleation in amyloid formation. *Chem. Commun.* **54**, 8667–8684
33. Hansen, C., Angot, E., Bergstrom, A. L., Steiner, J. A., Pieri, L., Paul, G., Outeiro, T. F., Melki, R., Kallunki, P., Fog, K., Li, J. Y., and Brundin, P. (2011) alpha-Synuclein propagates from mouse brain to grafted dopaminergic neurons and seeds aggregation in cultured human cells. *J. Clin. Invest.* **121**, 715–725
34. Vasili, E., Dominguez-Meijide, A., Flores-Leon, M., Al-Azzani, M., Kanellidi, A., Melki, R., Stefanis, L., and Outeiro, T. F. (2022) Endogenous levels of alpha-synuclein modulate seeding and aggregation in cultured cells. *Mol. Neurobiol.* **59**, 1273–1284
35. Vaikath, N. N., Erskine, D., Morris, C. M., Majbour, N. K., Vekrellis, K., Li, J. Y., and El-Agnaf, O. M. A. (2019) Heterogeneity in alpha-synuclein subtypes and their expression in cortical brain tissue lysates from Lewy body diseases and Alzheimer's disease. *Neuropathol. Appl. Neurobiol.* **45**, 597–608
36. Wang, Y., Shi, M., Chung, K. A., Zabetian, C. P., Leverenz, J. B., Berg, D., Srulijes, K., Trojanowski, J. Q., Lee, V. M., Siderowf, A. D., Hurtig, H., Litvan, I., Schiess, M. C., Peskind, E. R., Masuda, M., *et al.* (2012) Phosphorylated alpha-synuclein in Parkinson's disease. *Sci. Transl. Med.* **4**, 121ra120
37. Walker, D. G., Lue, L. F., Adler, C. H., Shill, H. A., Caviness, J. N., Sabbagh, M. N., Akiyama, H., Serrano, G. E., Sue, L. I., Beach, T. G., and Arizona Parkinson Disease, C. (2013) Changes in properties of serine 129 phosphorylated alpha-synuclein with progression of Lewy-type histopathology in human brains. *Exp. Neurol.* **240**, 190–204
38. Delenclos, M., Faroqi, A. H., Yue, M., Kurti, A., Castanedes-Casey, M., Rousseau, L., Phillips, V., Dickson, D. W., Fryer, J. D., and McLean, P. J. (2017) Neonatal AAV delivery of alpha-synuclein induces pathology in the adult mouse brain. *Acta Neuropathol. Commun.* **5**, 51
39. Tanaka, M., Collins, S. R., Toyama, B. H., and Weissman, J. S. (2006) The physical basis of how prion conformations determine strain phenotypes. *Nature* **442**, 585–589
40. Yamasaki, T. R., Holmes, B. B., Furman, J. L., Dhavale, D. D., Su, B. W., Song, E. S., Cairns, N. J., Kotzbauer, P. T., and Diamond, M. I. (2019) Parkinson's disease and multiple system atrophy have distinct alpha-synuclein seed characteristics. *J. Biol. Chem.* **294**, 1045–1058
41. Levin, J., Schmidt, F., Boehm, C., Prix, C., Botzel, K., Ryazanov, S., Leonov, A., Griesinger, C., and Giese, A. (2014) The oligomer modulator anle138b inhibits disease progression in a Parkinson mouse model even with treatment started after disease onset. *Acta Neuropathol.* **127**, 779–780
42. Limbocker, R., Staats, R., Chia, S., Ruggeri, F. S., Mannini, B., Xu, C. K., Perni, M., Cascella, R., Bigi, A., Sasser, L. R., Block, N. R., Wright, A. K., Kreiser, R. P., Custy, E. T., Meisl, G., *et al.* (2021) Squalamine and its derivatives modulate the aggregation of amyloid-beta and alpha-synuclein and suppress the toxicity of their oligomers. *Front. Neurosci.* **15**, 680026
43. Limbocker, R., Mannini, B., Ruggeri, F. S., Cascella, R., Xu, C. K., Perni, M., Chia, S., Chen, S. W., Habchi, J., Bigi, A., Kreiser, R. P., Wright, A. K., Albright, J. A., Kartanas, T., Kumita, J. R., *et al.* (2020) Trodusquemine displaces protein misfolded oligomers from cell membranes and abrogates their cytotoxicity through a generic mechanism. *Commun. Biol.* **3**, 435
44. Santos, J., Iglesias, V., Santos-Suarez, J., Mangiagalli, M., Brocca, S., Pallares, I., and Ventura, S. (2020) pH-dependent aggregation in intrinsically disordered proteins is determined by charge and lipophilicity. *Cells* **9**, 145
45. Uversky, V. N., Li, J., and Fink, A. L. (2001) Evidence for a partially folded intermediate in alpha-synuclein fibril formation. *J. Biol. Chem.* **276**, 10737–10744
46. McAllister, C., Karymov, M. A., Kawano, Y., Lushnikov, A. Y., Mikheikin, A., Uversky, V. N., and Lyubchenko, Y. L. (2005) Protein interactions and misfolding analyzed by AFM force spectroscopy. *J. Mol. Biol.* **354**, 1028–1042
47. Hoyer, W., Antony, T., Cherny, D., Heim, G., Jovin, T. M., and Subramaniam, V. (2002) Dependence of alpha-synuclein aggregate morphology on solution conditions. *J. Mol. Biol.* **322**, 383–393
48. Murray, I. V., Giasson, B. I., Quinn, S. M., Koppaka, V., Axelsen, P. H., Ischiropoulos, H., Trojanowski, J. Q., and Lee, V. M. (2003) Role of alpha-synuclein carboxy-terminus on fibril formation *in vitro*. *Biochemistry* **42**, 8530–8540
49. Gallardo, J., Escalona-Noguero, C., and Sot, B. (2020) Role of alpha-synuclein regions in nucleation and elongation of amyloid fiber assembly. *ACS Chem. Neurosci.* **11**, 872–879
50. Roeters, S. J., Iyer, A., Pletikapić, G., Kogan, V., Subramaniam, V., and Woutersen, S. (2017) Evidence for intramolecular antiparallel beta-sheet structure in alpha-synuclein fibrils from a combination of two-dimensional infrared spectroscopy and atomic force microscopy. *Sci. Rep.* **7**, 41051
51. Zhang, S., Liu, Y. Q., Jia, C., Lim, Y. J., Feng, G., Xu, E., Long, H., Kimura, Y., Tao, Y., Zhao, C., Wang, C., Liu, Z., Hu, J. J., Ma, M. R., Liu, Z., *et al.* (2021) Mechanistic basis for receptor-mediated pathological α-synuclein fibril cell-to-cell transmission in Parkinson's disease. *Proc. Natl. Acad. Sci. U. S. A.* **118**, e2011196118
52. Pujols, J., Pena-Diaz, S., Conde-Gimenez, M., Pinheiro, F., Navarro, S., Sancho, J., and Ventura, S. (2017) High-throughput screening methodology to identify alpha-synuclein aggregation inhibitors. *Int. J. Mol. Sci.* **18**, 478
53. Crespo, R., Villar-Alvarez, E., Taboada, P., Rocha, F. A., Damas, A. M., and Martins, P. M. (2016) What can the kinetics of amyloid fibril formation tell about off-pathway aggregation? *J. Biol. Chem.* **291**, 2018–2032
54. Diaz-Caballero, M., Navarro, S., Fuentes, I., Teixidor, F., and Ventura, S. (2018) Minimalist prion-inspired polar self-assembling peptides. *ACS Nano* **12**, 5394–5407
55. Volpicelli-Daley, L. A., Luk, K. C., and Lee, V. M. (2014) Addition of exogenous alpha-synuclein preformed fibrils to primary neuronal cultures to seed recruitment of endogenous alpha-synuclein to Lewy body and Lewy neurite-like aggregates. *Nat. Protoc.* **9**, 2135–2146